

Near-IR spectroscopic ages of massive star clusters in M82.

A. Lançon¹, J.S. Gallagher, III², M. Mouhcine³, L.J. Smith^{4,5}, D. Ladjal⁶, and R. de Grijs^{7,8}

¹ Observatoire Astronomique de Strasbourg, Université L. Pasteur & CNRS (UMR 7550), Strasbourg, France

² Department of Astronomy, University of Wisconsin-Madison, WI, USA

³ Astrophysics Research Institute, Liverpool John Moores University, UK

⁴ Space Telescope Science Institute and European Space Agency, Baltimore, MD, USA

⁵ Department of Physics and Astronomy, University College London, London, UK

⁶ Institute of Astronomy, Katholieke Universiteit, Leuven, Belgium

⁷ Department of Physics & Astronomy, The University of Sheffield, Sheffield, UK

⁸ National Astronomical Observatories, Chinese Academy of Sciences, Beijing, China

Received 20/01/08 - Accepted 10/04/08

ABSTRACT

Context. Like other starburst galaxies, M 82 hosts compact, massive ($> 5 \times 10^5 M_{\odot}$) young star clusters that are interesting both in their own right and as benchmarks for population synthesis models.

Aims. In addition to assessing or reassessing the properties of some of the brightest near-IR sources in M 82, this paper addresses the following questions. Can population synthesis models at $\lambda/\delta\lambda \simeq 750$ adequately reproduce the near-IR spectral features and the energy distribution of these clusters between 0.8 and $2.4 \mu\text{m}$? How do the derived cluster properties compare with previous results from optical studies?

Methods. We analyse the spectra of 5 massive clusters in M 82, using data acquired with the spectrograph SpeX on the InfraRed Telescope Facility (NASA/IRTF) and a new population synthesis tool with a highly improved near-IR extension, based on a recent collection of empirical and theoretical spectra of red supergiant stars.

Results. We obtain excellent fits across the near-IR with models at quasi-solar metallicity and a solar neighbourhood extinction law. Spectroscopy breaks a strong degeneracy between age and extinction in the near-IR colours in the red supergiant-dominated phase of evolution. The estimated near-IR ages cluster between 9 and 30 Myr, i.e. the ages at which the molecular bands due to luminous red supergiants are strongest in the current models. They do not always agree with optical spectroscopic ages. Adding optical data sometimes leads to the rejection of the solar neighbourhood extinction law. This is not surprising considering small-scale structure around the clusters, but it has no significant effect on the near-IR based spectroscopic ages.

Conclusions. The observed IR-bright clusters are part of the most recent episode of extended star formation in M 82. The near-IR study of clusters that are too faint for optical observation adds important elements to the age distribution of massive clusters in dusty starbursts. Further joint optical and near-IR spectroscopic studies will provide strong constraints on the uncertain physics of massive stars on which population synthesis models rest.

Key words. Galaxies: individual: M 82 – Galaxies: star clusters – Galaxies: stellar content – Galaxies: starburst – Infrared: galaxies – Stars: supergiants

1. Introduction

Starburst galaxies host large populations of star clusters, and it has become increasingly clear that global star formation processes and cluster formation processes are intimately linked (Meurer et al. 1995, Larsen 2006, Elmegreen 2006). This is an important motivation for detailed studies of young star clusters, their distributions in terms of mass and age, their mass-to-light ratios and their stellar initial mass functions.

Because star formation originates in molecular clouds, starburst galaxies tend to be dusty, and young star clusters can be

severely obscured. As beautifully illustrated by near-IR and optical Hubble Space Telescope (HST) images of galaxies such as M 82 or the Antennae (de Grijs et al. 2001, Alonso-Herrero et al. 2003, McCrady et al. 2003, Rossa et al. 2007), the brightest near-IR star clusters can go undetected at optical wavelengths, and vice-versa. Optical studies tend to focus on lines of sight through holes in the dust, and the derived distributions of cluster properties are subject to biases. In order to obtain a more complete picture of the cluster populations, it seems crucial to combine optical and near-IR data. This can be done with multi-band photometry or with spectroscopy.

The importance of near-IR spectroscopy in studies of dusty star forming galaxies has long been recognised (Rieke &

Lebofsky 1979), and spectra in the H or K windows have been used to constrain star formation histories (e.g. Rieke et al. 1993, Oliva et al. 1995, Lançon & Rocca-Volmerange 1996, Satyapal et al. 1997, Förster Schreiber et al. 2001).

However, near-IR studies of young stellar populations remain difficult. Among the relevant problems are the following (see main text for details and references).

(i) Evolutionary tracks for massive stars are uncertain, in particular in the red supergiant phase which is the predominant source of near-IR light at ages of order 10^7 yr.

(ii) Model atmospheres for luminous red supergiants are not yet reliable, and this affects the mapping of isochrones into colour diagrams.

(iii) The stellar population of a cluster is stochastic, and the intrinsically small number of bright stars leads to potentially large spreads and systematics in the expected cluster properties.

(iv) The subtraction of very irregular starburst galaxy backgrounds can be hazardous.

(v) It matters to photometric studies that the shape of the dust attenuation law depends on the unknown spatial distribution of the dust as well as on the nature of the dust; there are degeneracies in colours, for instance between age and extinction.

As a result of some or all of the above, discrepancies between photometric studies that do or do not include near-IR passbands can occur. The consistency between results obtained from near-IR and from optical spectroscopic data needs to be tested.

With *extended* spectroscopy of massive star clusters, by which we mean spectroscopy that extends through optical and near-IR wavelengths, it becomes possible to isolate some of the above aspects. By using stellar absorption features exclusively, dust attenuation issues are mostly eliminated. By focusing on very massive star clusters, stochasticity effects can be kept below acceptable levels. Contamination by other stellar populations on neighbouring lines of sight remains an issue in crowded areas, but can be addressed with multicomponent models, more safely with spectroscopy than with photometry. In the end, the spectroscopic analysis is mostly sensitive to the ingredients of the population synthesis models, such as the stellar evolution tracks and the stellar spectra assigned to each point along these tracks. One may expect two types of results. If the best-fit models based on the near-IR data are not consistent with the optical data, this points to inadequacies of the input physics of the models, i.e. likely systematic errors in both optical and near-IR cluster ages. Conversely, a good fit to the optical and near-IR data set will provide significantly more robust cluster properties than a fit to a single spectral window or to photometric data.

In this paper, we analyse extended spectra of five massive clusters in the nearby starburst galaxy M82, using a population synthesis tool with a highly improved near-IR spectroscopic extension. We show that it is possible to obtain a good representation of all the near-IR features ($0.8\text{-}2.4\ \mu\text{m}$, $\lambda/\delta\lambda \sim 750$). We investigate whether the near-IR results are consistent with the optical constraints, and what we can learn about extinction and the possible origins of difficulties faced in photometric age-dating procedures.

Section 2 introduces the new population synthesis tool. In Sections 3 and 4 we describe and analyse the spectra of star clusters in M82. Selected aspects of the analysis as well as the issue of stochastic fluctuations are discussed in Sect. 5. Conclusions are summarised in Sect. 6.

2. Synthetic near-IR spectra of young stellar populations

Multi-wavelength spectroscopic studies of young stellar populations have been limited by the absence of complete stellar spectral libraries with adequate near-IR coverage and resolution. A reasonable coverage of the HR diagram was available in the libraries of Pickles (1998) and Lejeune et al. (1998). Both have insufficient spectral resolution for our current purposes and lack some of the most important molecular features of cool stars, in particular between 0.9 and $1.5\ \mu\text{m}$. Libraries at higher spectral resolution are usually limited to selected near-IR spectral windows and their continua have sometimes been normalised (Meyer et al. 1999, Wallace et al. 2000, Cenarro et al. 2001, Ivanov et al. 2004 and further references therein). Unfortunately, many of the near-IR features of interest for population diagnostics are broad molecular bands that can not be studied reliably when the spectra in the traditional windows of ground based observations are acquired separately (unless high quality absolute flux calibration is achieved).

An exception has been the collection of spectra of cool stars of Lançon & Wood (2000), which covers wavelengths from 0.5 to $2.4\ \mu\text{m}$. They allowed Mouhcine & Lançon (2002) and Maraston (2005) to produce extended synthetic single stellar population spectra (SSP spectra) with a near-IR resolution $R = \lambda/\delta\lambda \sim 1000$. That work focused on intermediate age populations, in which O-rich and C-rich TP-AGB stars are the predominant sources of near-IR light. Only a handful of red supergiant spectra were available at the time. The synthetic spectra presented here represent an important step towards a more robust extension of previous work to ages between 5 Myr and a few 100 Myr.

2.1. New input spectra

The models in this paper use the empirical spectra of luminous red stars that were compared with theoretical spectra by Lançon et al. (2007 a; hereafter LHLM07). They were acquired in part with CASPIR on the 2.3m Telescope of the Australian National University (McGregor et al. 1994), in part with SpeX on NASA's InfraRed Telescope Facility (Rayner et al. 2003). All the spectra cover wavelengths from 0.9 to $2.4\ \mu\text{m}$ continuously, at $\lambda/\delta\lambda \geq 750$ (the SpeX data extend to $0.81\ \mu\text{m}$). The flux calibration through this wavelength range has been achieved using warm stars with known photometry. We refer to Lançon & Wood (2000) and Vacca et al. (2003) for the calibration methods applied respectively to the CASPIR and the SpeX data.

The theoretical spectra available to LHLM07 were computed with the PHOENIX code (P. Hauschildt and collaborators), for a metallicity typical of the sun but with surface abundances

of C, N and O modified according to expectations from stellar evolution calculations. We refer to that article for a more complete description. The authors also describe and discuss the minimum- χ^2 procedure used to estimate the effective temperature (T_{eff}), the surface gravity g and the extinction A_V of individual stars. The adopted extinction law is taken from Cardelli et al. (1989), with $R_V = 3.1$.

The conclusions of LHLM07 most relevant to near-IR synthesis at $R \sim 1000$ are the following: theoretical spectra *are* able to reproduce those of static red giants down to effective temperatures of about 3500 K; the models available to the authors *did not* as yet provide a satisfactory match of the spectra of cool and luminous red supergiants, even when the effects of internal mixing on surface abundances had been taken into account. Further theoretical work is being undertaken to improve the supergiant models; as yet, using theoretical spectra directly for population synthesis purposes is considered premature.

In order to build a suitable library for population synthesis purposes, the red supergiants and bright giants of the observed sample were subdivided into subsets of stars of class Ia, class Iab and class Ib/II. Each subset was sorted according to estimated T_{eff} . Bins in T_{eff} were then constructed, containing between 1 and 5 stars depending on the number of spectra available in a given T_{eff} range, and depending on the individual quality of those data. The spectra in each bin were examined individually, and compared with spectra in neighbouring bins and in neighbouring luminosity classes. This had the purpose of removing or reclassifying outliers, in order to obtain sequences along which spectral features evolve reasonably regularly. It must be kept in mind that, since synthetic spectra cannot reproduce the empirical spectra well, a large uncertainty affects estimated parameters such as T_{eff} or $\log(g)$. Therefore, there is indeed quite some freedom for adjustment, especially for temperatures below 3800 K and for stars of class Ia and Iab.

The spectra within a given bin were then dereddened and averaged. All observed spectra cover wavelengths between 0.97 and 2.4 μm but only some extend to shorter wavelengths. Our bin averages all reach 0.51 μm : the best fitting model was used to extend the data in bins where no empirical short wavelengths spectra were available.

The resulting sequences have lower estimated values of $\log(g)$ for more luminous stars, as expected. The assigned values depend strongly on the assumed value of the microturbulence parameter in the stellar models. When using microturbulent velocities of only 2 or 3 km.s^{-1} (LHLM07), the stars of class Ia are assigned a value of $\log(g)$ of -1 , i.e. a value that is not reached by standard sets of evolutionary tracks. With higher microturbulent velocity parameters (as suggested e.g. by studies of Tsuji et al. 1976, Gray et al. 2001, Origlia et al. 1993, 1997), $\log(g)$ rises to -0.5 or 0 for the same class Ia spectra, and the spectral fits tend to improve (Lançon et al. 2007 b). We have taken this trend into account qualitatively to locate the sequences in Fig. 1. At the time of this work, the grid of large microturbulence models has too coarse a sampling in T_{eff} to allow us to also reassign temperatures consistently. This is an additional reason for uncertainty in the T_{eff} values along the sequences of average spectra.

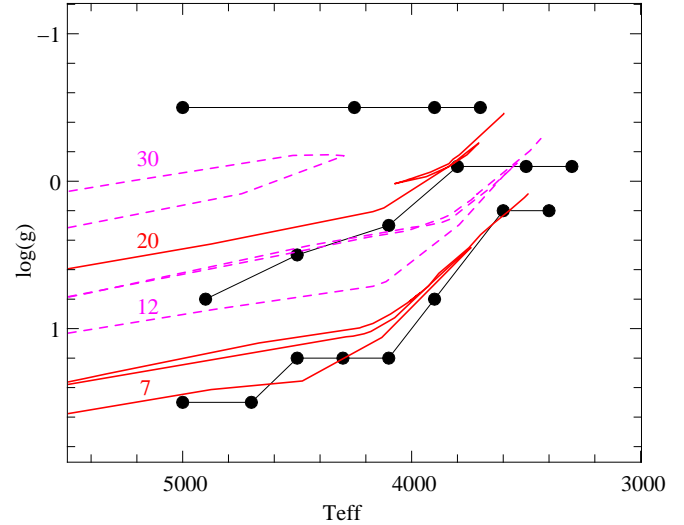


Fig. 1. Temperatures (K) and gravities (cm.s^{-2}) assigned to the average spectra of stars of luminosity class Ia (lowest gravities), Iab (intermediate gravities), and Ib/II (highest gravities). Overplotted are the evolutionary tracks of Bressan et al. (1993) for the indicated stellar initial masses (in units of M_{\odot}).

A procedure similar to the one just described has been applied (with much smaller uncertainties on the stellar parameters) to the empirical giant star spectra analysed by LHLW07. Together with the average spectra of long period variables and carbon stars of Lançon & Mouhcine (2002), this provides us with a library suitable for the construction of SSP spectra at both young and old ages. Details about the modelling of the older populations lie outside the scope of the present article.

2.2. Population synthesis assumptions and predictions

The synthesis of SSP spectra is performed with a version of the code PÉGASE.2 (Fioc & Rocca-Volmerange 1997, 1999)¹ that has been adapted to our purposes following Mouhcine & Lançon (2002). The computation of isochrones from evolutionary tracks is unchanged, but red supergiant phases are flagged². Non-flagged points along the isochrones are represented with spectra of the default library of PÉGASE.2, i.e. the semi-empirical library of Lejeune et al. (1998). Flagged points are represented with the new average spectra of red supergiants described above. The bolometric corrections needed to scale the fluxes are computed by forcing the near-IR spectra to match the level of the Lejeune spectra in the J band. Other options for the bolometric corrections have not yet been explored. For the linear interpolation between the spectra of the three red supergiant sequences, we choose to proceed as follows: first we interpolate along each of the two bracketing sequences to reach the target T_{eff} , then we interpolate between the two resulting spectra according to $\log(g)$.

The stellar evolution tracks used in this paper are taken from Bressan et al. 1993. Our study is limited to near-solar

¹ cf. <http://www2.iap.fr/pegase/>

² Red giant and asymptotic red giant phases are also flagged but this is relevant only to intermediate age and old populations.

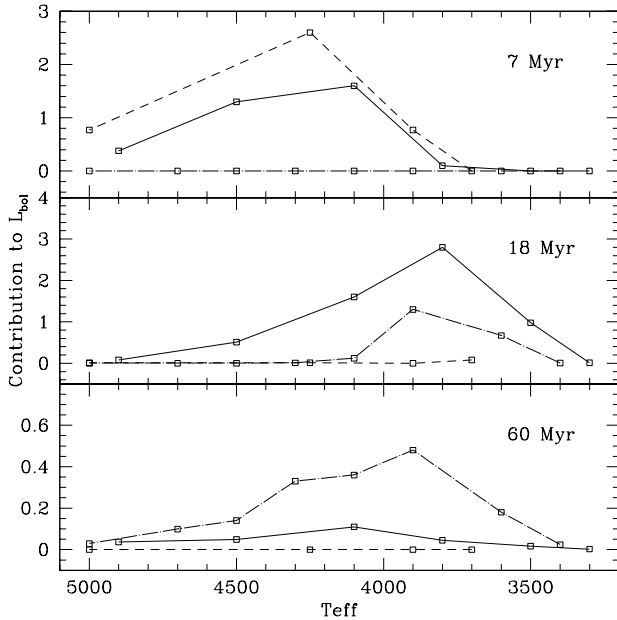


Fig. 2. Contributions of the spectra of supergiants of class Ia (dotted), Iab (solid) and Ib/II (dashed) to the bolometric luminosity. The contributions are average absolute values, in L_{\odot} , and are given scaled to a total initial stellar mass of $1 M_{\odot}$ (Salpeter IMF extending from 0.1 to $120 M_{\odot}$).

metallicity (tracks at $Z=0.02$) and we use the IMF of Salpeter (1955) unless otherwise stated. Any star initially more massive than $7 M_{\odot}$ is flagged as a supergiant when it evolves off the main sequence. As a consequence, the new collection of supergiant spectra modifies the predictions of PÉGASE up to an age of about 75 Myr.

Figure 2 indicates which of the average red supergiant spectra contribute most strongly to the bolometric light of single-age populations at any given ages. Spectra of the class Ia sequence are dominant (among red supergiants) only at the youngest ages (7-8 Myr). Their contribution becomes negligible after about 15 Myr, but we note that this number is particularly sensitive to the value of the gravity assigned to the stars observed. Stars of class Iab are dominant between ages of about 10 and about 25 Myr. Afterwards, the strongest red supergiant contributions to L_{bol} come from stars of class Ib/II.

The red supergiants all together are responsible for 70–85% of the $2 \mu\text{m}$ flux and 45–75% of the $1 \mu\text{m}$ flux, on average, at ages between 9 Myr and 65 Myr (see Sect. 5.2). Stars hotter than 5000 K provide the rest of the emission. Because the library of Lejeune et al. (1998) has a low resolution in the near-IR, our models will lack the high resolution spectral features of the warmer stars, and this is a caveat in particular at short wavelengths. For the main molecular bands in the H and K windows, implications are limited. Stars warmer than 5000 K have very little CO absorption at $1.6 \mu\text{m}$ and their contributions at $2.3 \mu\text{m}$ remain small.

As it can be seen in Fig 3, the new spectra do not only improve the spectral resolution but they also modify the energy distribution. With the adopted bolometric corrections (forced

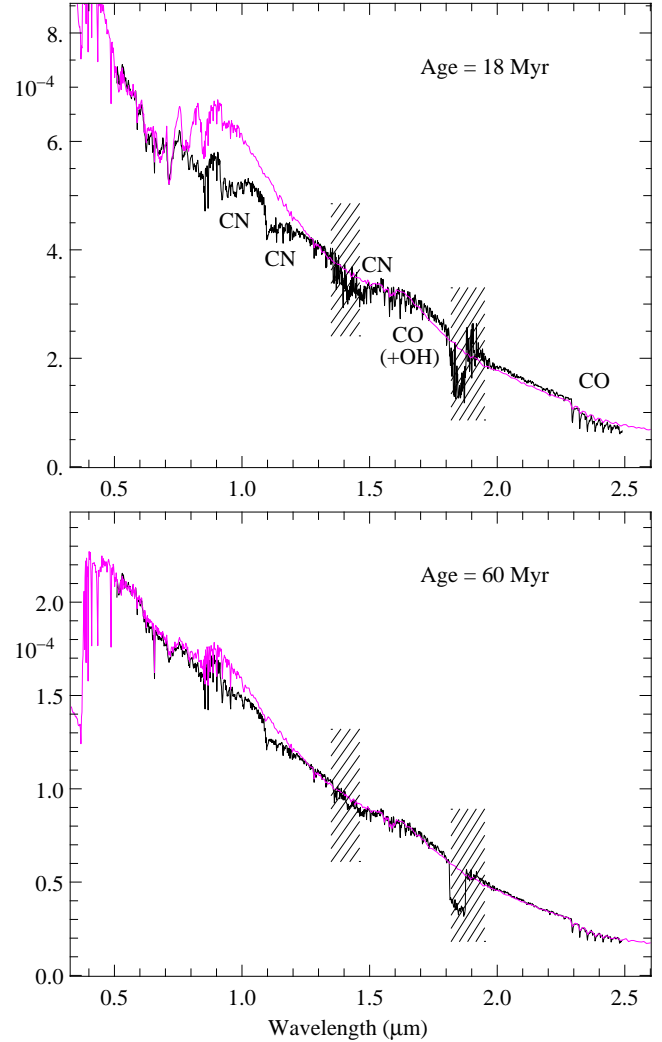


Fig. 3. Comparison of the new model spectra of single-age populations (higher spectral resolution) with the standard predictions of PÉGASE.2 (lower spectral resolution). The spectra have been reddened for display (top: $A_V=1$, bottom: $A_V=1.5$), and are presented in arbitrary units of energy per unit wavelength. Regions of low signal-to-noise ratio and partly missing data are shaded.

match with the old models in the J band), the J, H and K magnitudes are not changed significantly, but the flux around $1 \mu\text{m}$ is strongly modified for ages between 10 and 25 Myr. The molecular bands of CN (e.g. $1.1 \mu\text{m}$, $1.4 \mu\text{m}$) were not present at an appropriate level in the theoretical models that entered the semi-empirical library of Lejeune et al. (1998).

3. Observations and the M82 Cluster Sample

3.1. Observations

Near-IR spectra of the nucleus and of five star clusters in M 82 were acquired with the infrared spectrograph SpEX (Rayner et al. 2003) mounted on the NASA Infrared Telescope Facility (IRTF), as detailed in Table 1. The targets were selected to be among the brightest near-IR sources in M 82. They are iden-

Table 1. Observations of star clusters in M82

Target	Date (d/m/yr)(UT)	Usable time on target	P.A.
L & F	31/3/02	2 × 120 s	22°
1a & 1c	3/4/02	2 × 240 s	125°
z	3/4/02	3 × 240 s	125°
nucleus	3/4/02	4 × 240 s	22°

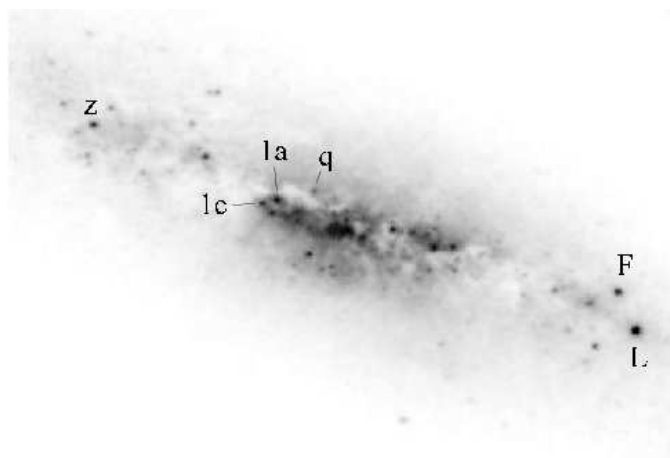


Fig. 4. Bright near-IR star clusters in the inner disc of M82. Shown in inverted greyscale are two merged HST/NICMOS3 narrow H band archive images (filter F164N; HST program 7218, P.I. Rieke). The clusters discussed in the present article are labelled following the nomenclature of McCrady et al. (2003) and McCrady & Graham (2007).

tified in Figure 4, following the nomenclature of McCrady & Graham (2007).

The short wavelength setting of the SpeX instrument covers wavelengths from 0.81 to 2.4 μm in a single observation, thus eliminating some of the uncertainties inherent in the relative flux calibration of independent observations in the Z, J, H and K windows. Since many of the spectral features of interest are broad molecular bands that extend across the “forbidden” regions of high telluric absorption (telluric H₂O around 1.15, 1.4 and 1.9 μm), this is a significant advantage of SpeX over many other current instruments.

Observing conditions were not photometric, and as a compromise between spectral resolution and the need to collect photons, we used a 0.8'' × 15'' slit, giving a resolving power of $R = 750$. A fraction of the red supergiant stars were observed during the same run, with the same instrumental setting.

The targets were observed with SpeX in a series of individual exposures of 120 s or 240 s. Sky exposures were obtained for each frame at 140'' to the South-East of the target position, well outside the main body of the galaxy. Several A0 type stars with known photometry were observed for the relative flux calibration and for the correction of telluric absorption (Vacca et al. 2003). In the end, the observations of the A0V star HD 92738 provided the best telluric correction for all the targets in M82. The data reduction was based on the instrument-

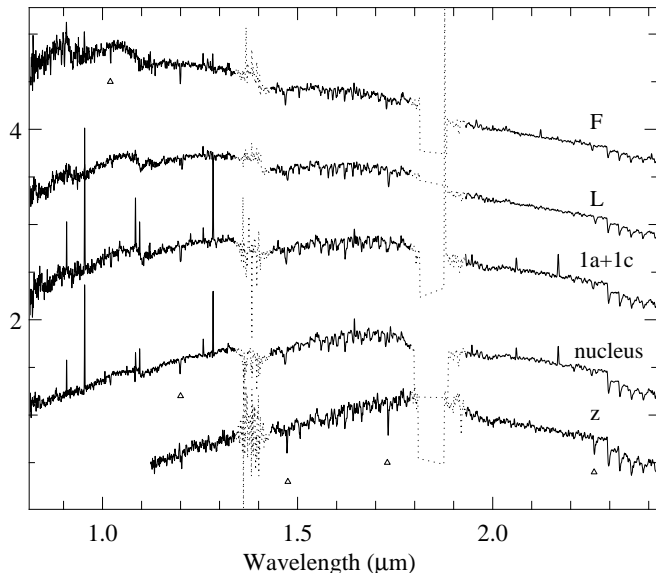


Fig. 5. IRTF/SpeX spectra of the observed star clusters in M82. The nuclear spectrum is also shown for reference. The data are normalised to unit average flux density (energy per unit wavelength) in the H band, and offset for clarity (the zero flux line holds for cluster z). They have been smoothed slightly for display. Triangles indicate bad pixels. Dotted spectral segments are regions of low signal-to-noise ratio (residuals of the telluric correction) or missing data.

Table 2. Summary of M82 Cluster Properties

Cluster	Age (optical) (Myr)	Dynamical Mass (10 ⁵ M _⊙)	Age (IR) (Myr)
F	40–80 ^{1,2,3}	4.7–13 ^{2,3,4}	15–50
L	≈ 60 ¹	34–46 ⁴	10–35
1a	6–7 ⁵	7.6–9.6 ⁴	9–25
1c		4.4–6.0 ⁴	9–25
z		4.7–9.45 ⁶	10–30

References: 1. Gallagher & Smith (1999); 2. Smith & Gallagher (2001); 3. Bastian et al. (2007); 4. McCrady et al. (2007); 5. Smith et al. (2006); 6. see text.

specific software package, Spextools, version 3.1 (Cushing et al. 2004). This software offers the possibility of rescaling the spectral segments of various orders after they have been flux calibrated and before they are merged. But, as expected when the calibration is successful, we found no need to apply such an order-dependent scaling factor.

The final merged spectra are shown in Fig. 5. They are available from the authors upon request.

3.2. The M82 Cluster Sample

We now describe previous optical studies of our cluster sample; a summary of their derived ages and masses is given in Table 2.

Clusters M82-F and M82-L are located in the western disc outside the main star forming region. They have been studied

previously using optical spectra that extended to about 9000 Å, and high resolution images (Gallagher & Smith 1999; Smith & Gallagher 2001; McCrady et al. 2005, Smith et al. 2006, Bastian et al. 2007). Cluster F is intrinsically fainter than L but is seen through a lower optical depth of dust: it appears brighter than L in the V band but fainter in K. Based on optical spectra the age favoured for cluster F lies between 40 and 80 Myr (Gallagher & Smith 1999, Smith & Gallagher 2001, Bastian et al. 2007). Dynamical mass estimates range from $4.7 \cdot 10^5$ to $13 \cdot 10^5 M_{\odot}$ (Smith & Gallagher 2001; Bastian et al. 2007; McCrady et al. 2007). The low mass-to-light ratio of cluster F has been used to infer a top-heavy IMF (Smith & Gallagher 2001).

The optical spectra of cluster L indicate a similar age (around 60 Myr). McCrady et al. (2007) find a dynamical mass as high as $34\text{--}46 \cdot 10^5 M_{\odot}$ for this cluster.

Clusters M82-1a (labeled A1 in Smith et al. 2006) and M82-1c are located less than $1''$ apart at the edge of the main star forming region in the inner eastern disc (region A of O’Connell & Mangano, 1978), in an area surrounded by very thick lanes of dust. The optical spectroscopic age of cluster 1a is 6–7 Myr, i.e. significantly younger than that of L and F. No spectroscopic age is available for cluster 1c to our knowledge. Photometric masses for cluster 1a range from $6.4 \cdot 10^5$ to $18 \cdot 10^5 M_{\odot}$ depending on the adopted stellar initial mass function (Smith et al. 2006). Dynamical masses have values of $7.6\text{--}9.6 \cdot 10^5 M_{\odot}$ for cluster 1a and $4.4\text{--}6.0 \cdot 10^5 M_{\odot}$ for cluster 1c (McCrady et al. 2007).

Cluster M82-z is located in the eastern disc region known as region B (O’Connell & Mangano 1978). It is not mentioned in the optically selected cluster list for this region by de Grijs et al. (2001), and is also absent in the *U*-band selected cluster sample studied by Smith et al. (2007). Indeed, cluster *z* is barely detected at F555W in the HST/ACS Wide Field Channel mosaic of M82 (Mutchler et al. 2007).

The high near-IR brightness of cluster *z* suggests that the cluster may be in the red supergiant-dominated phase of evolution, i.e. that it might be one of the youngest clusters in region B. Smith et al. (2007) find that the peak epoch of cluster formation in this region was ~ 150 Myr ago, with clusters forming at a lower rate until 12–20 Myr ago. To estimate the dynamical mass of cluster *z*, we combined the velocity dispersion measurement of McCrady et al. (2007) with a new radius measurement on the F814W image from the ACS mosaic of M82 (Mutchler et al. 2007; measurement by I. Konstantopoulos, private communication). We found a mass range of $4.7\text{--}9.5 \cdot 10^5 M_{\odot}$.

4. Near-IR analysis

4.1. Fitting procedure

The relative quality of the model fits to the near-IR spectrum of a given cluster is measured with a reduced χ^2 .

$$\chi^2 = \frac{1}{N} \sum_i W_i \frac{(S_i - \alpha M_i)^2}{\sigma_i^2}$$

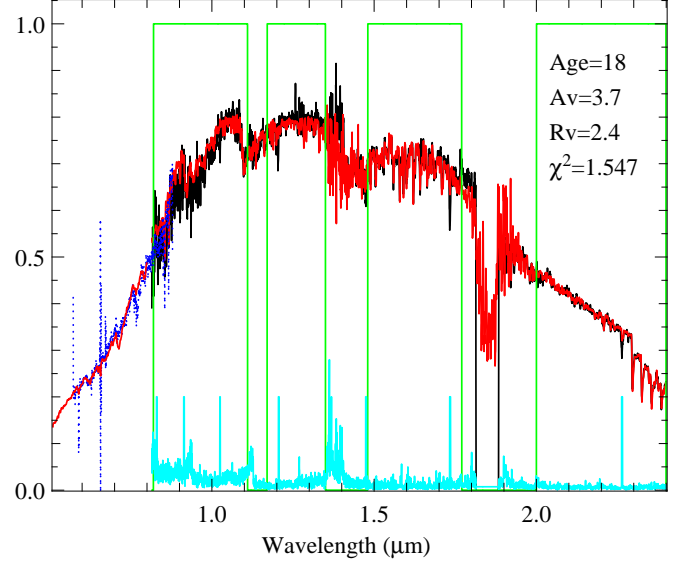


Fig. 6. Best fit to the near-IR spectrum of cluster M82-L (arbitrary units of energy per unit wavelength). The model (grey; red in the electronic version) follows the SpeX data (black) very closely over the whole range of that data (0.81–2.4 μm). It also matches the optical observations of Smith & Gallagher (2001; dotted) if one adopts $R_V \approx 2.4$ for the extinction law. Wavelengths outside the rectangular boxes have zero weight in the χ^2 -minimisation procedure. The noise spectrum used to weight the χ^2 is shown in light grey (cyan in the electronic version).

where i runs through the spectral pixels, S is the empirical spectrum, M the model under study, α the factor that minimises χ^2 for this model, and σ the estimated noise. W is set to either 0 or 1. $W = 0$ is used to mask regions where strong telluric absorption leaves strong residuals after correction. W also allows us to perform fits on selected, restricted wavelength ranges. N is the number of pixels with $W = 1$. The value of χ^2 is useful only to compare the quality of various model fits to a given spectrum. Note that it does not fulfill the mathematical requirements (such as statistical independence of the data points) that would allow us to interpret its numerical values in terms of likelihoods.

The models considered are SSPs with ages between 1 and about 100 Myr, reddened using the family of extinction laws of Cardelli et al. (1989). The shape of these laws at near-IR wavelengths ($>0.9 \mu\text{m}$) is independent of the adopted value of $R_V = A_V/E(B-V)$. Therefore, the estimated near-IR age is independent of R_V . Constraints on R_V are obtained when optical data are added to the near-IR spectrum. The estimated intrinsic (dereddened) luminosity of the cluster will be affected by the assumptions on the extinction law much more than the cluster ages.

4.2. Cluster L

Figure 6 shows the best fit to the near-IR spectrum of cluster L, together with optical extensions of the models and the data. The best-fit age is 18 Myr. Figures 7 and 8 show zooms on subsets

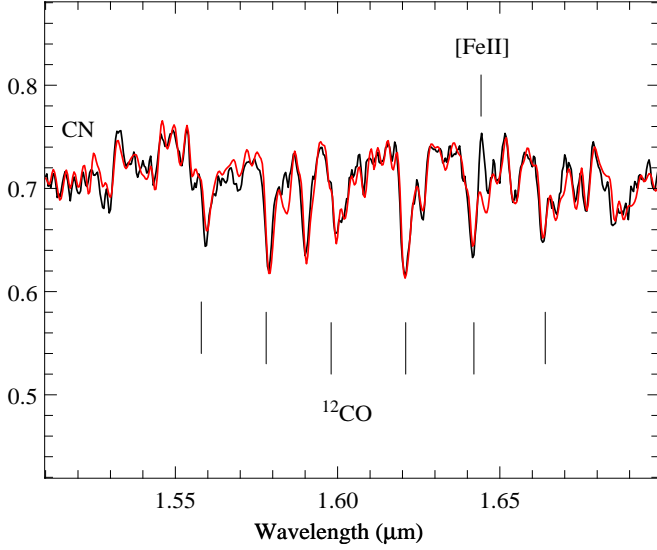


Fig. 7. Zoom on the H band of the fit of Fig. 6 (no additional renormalisation was required). The fit allows for a good measurement of the [FeII] emission line.

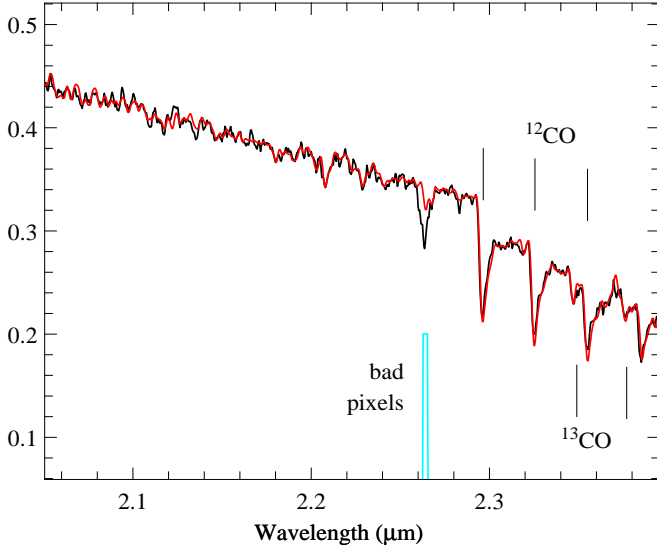


Fig. 8. Zoom on the K band of the fit of Fig. 6 (no additional renormalisation was required).

of the spectrum: the fit quality is excellent. In particular, this fit would provide an excellent background subtraction for the measurement of nebular emission lines on the line of sight to the cluster. The extinction law of Cardelli et al. (1989) leads to a very satisfactory representation of the near-IR energy distribution of the cluster, and with $R_V=2.4-2.7$ the fit extends down to 6000 \AA .

The χ^2 -map of Fig. 9 shows a valley that illustrates the degeneracy between age and extinction present in the colours of SSPs. The depth of the valley (solid curve in the lower graph of that figure) measures the quality of the fit to the spectral absorption features, together with residual effects in the reddening-corrected energy distribution. Separate fits to subset of the data provide a handle on uncertainties, and have the additional advantage of being less sensitive to the actual shape of

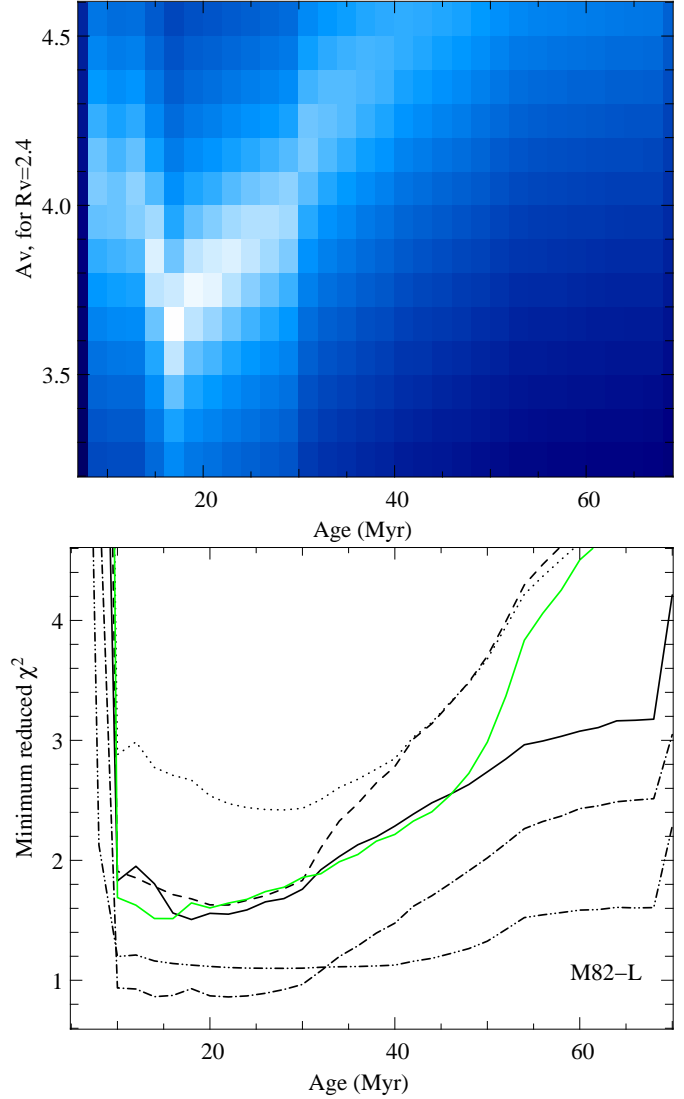


Fig. 9. Minimum χ^2 as a function of age for cluster L. **Solid:** fit performed using the full range of wavelengths, with weights as indicated in Fig. 6. The upper graph shows the χ^2 valley in the Age-Extinction plane for this case. **Dashed:** wavelengths restricted to the H+K windows. **Dotted and dot-dashed:** wavelengths restricted to only the H window and only the K window. **Dot-dot-dashed:** wavelengths below $1.35 \mu\text{m}$ only. **Thick solid, green (or grey):** fit to the full wavelength range but with a modified extinction law.

the adopted extinction law. The figure shows that the age ranges found in these tests overlap nicely, globally favouring ages between 10 and 35 Myr. Note that the lower signal-to-noise ratio below $1.35 \mu\text{m}$ leads to a very shallow χ^2 minimum in the corresponding curve. One final test was performed using the full wavelength range available, but allowing the extinction law to be modified by multiplication with a second order polynomial. Acceptable changes in the energy distribution were found to be limited to less than $\sim 5\%$, and the resulting age range was not significantly affected. The value of R_V providing the best match to the global energy distribution correlates with age: $R_V \approx 3.1$ is found for ages near 10 Myr, $R_V < 3.1$ for older ages.

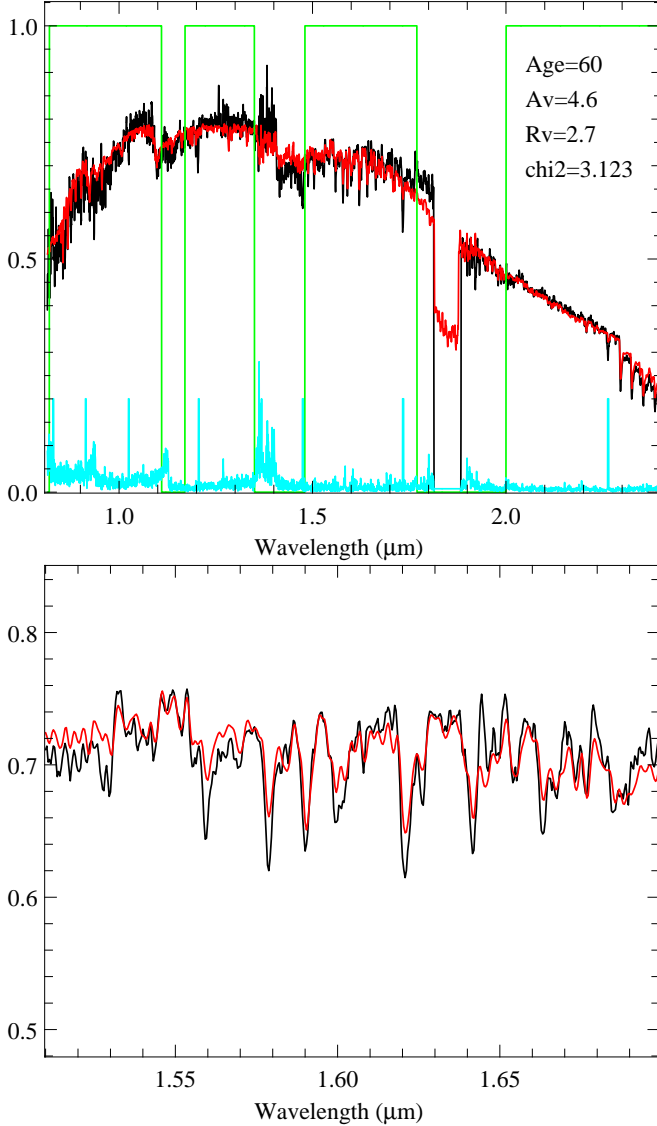


Fig. 10. Cluster L: Best fit to the near-IR spectrum and the global energy distribution when the age is *assumed* equal to 60 Myr.

For the sake of completeness, Figure 10 shows the best fit obtained assuming an age of 60 Myr, i.e. the age suggested by recent studies of the spectrum at wavelengths shorter than $1 \mu\text{m}$: although the energy distribution can be matched decently (with $R_V=2.7$), the fits to the molecular bands are poor. Within the framework of the set of SSP models described above (i.e. the new library of red supergiant spectra, the current estimate of the parameters of the library stars and the adopted set of stellar evolution tracks), an age of 60 Myr is excluded. We refer to Sect. 5 for a further discussion of model-dependence.

4.3. Cluster F

For cluster F, the best fit to the near-IR spectrum as a whole is obtained for ages around 35 Myr. The best model provides an excellent representation of the spectral features longwards of $1.06 \mu\text{m}$, and a good representation of the CN bands at

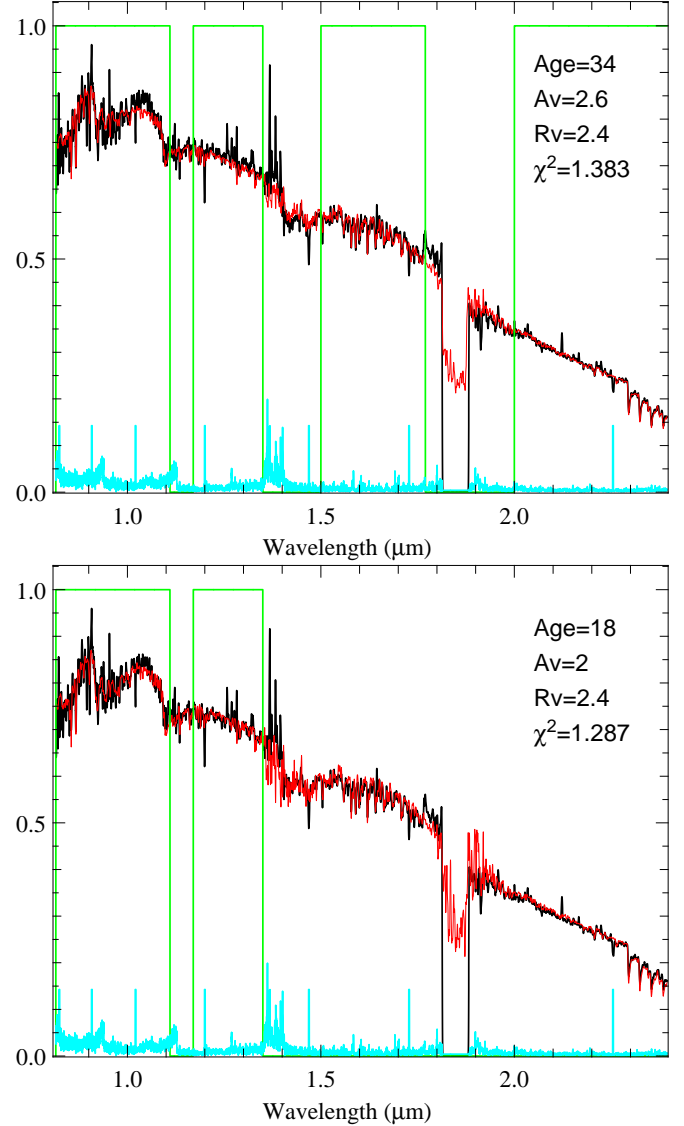


Fig. 11. Best fit to the near-IR spectrum of cluster M82-F. For the bottom graph, only wavelengths below $1.35 \mu\text{m}$ have been used to constrain the fit. The data and the model have been smoothed with a gaussian kernel for display (FWHM= 13 \AA), and the plotted noise spectrum takes this smoothing into account.

shorter wavelengths (Fig. 11). This is confirmed by fits to individual near-IR wavelength windows (Fig. 12). The H and K band spectra alone indicate ages of 30-40 Myr. A restriction to wavelengths below $1.35 \mu\text{m}$ favours slightly younger ages, at which SSP models display deeper CN features, and a correspondingly lower extinction (we recall that R_V affects the value of A_V but not the quality of the fit at wavelengths $> 0.9 \mu\text{m}$). The bottom panel of Fig. 11 illustrates how well this younger model still reproduces the global energy distribution of cluster F. The age-extinction degeneracy is almost perfect: near-IR broad band colours alone could not have provided significant constraints on either the age or the amount of reddening within the age range of interest.

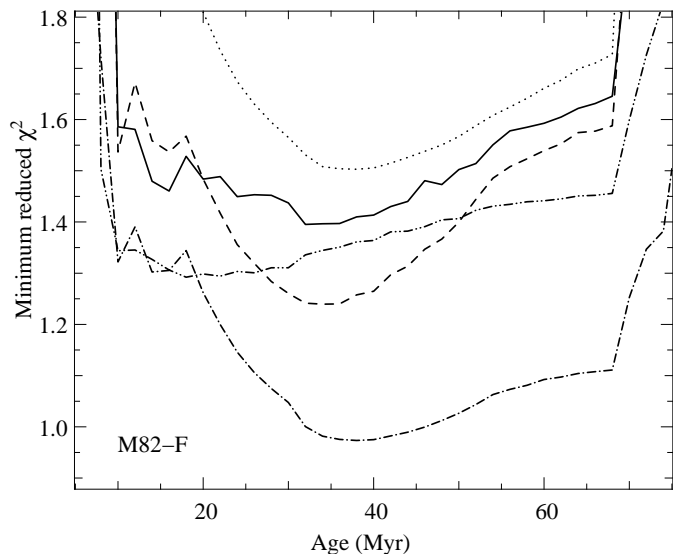


Fig. 12. χ^2 versus model age for cluster F. Compare with Fig. 9.

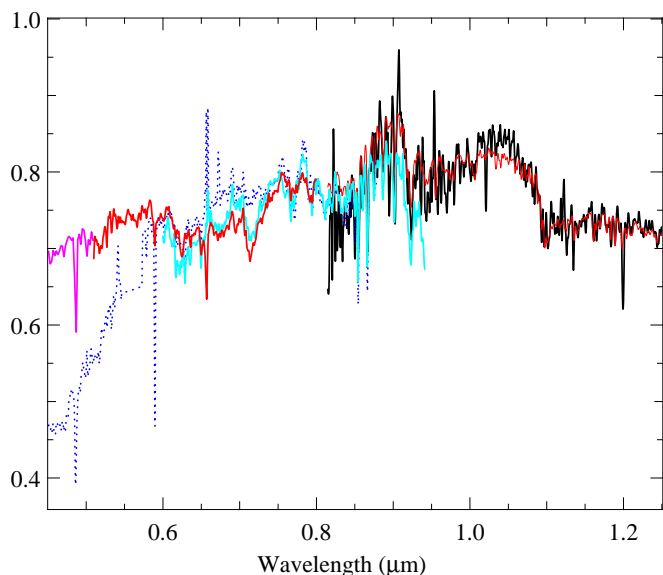


Fig. 13. Cluster F. Same as top panel of Fig. 11, but with available optical spectra superimposed (Age=34 Myr, $R_V=3.3$ for best match to the STIS data). The solid cyan (light grey) extension to optical wavelengths is the HST/STIS spectrum of Smith et al. (2006), and the dotted curve is the WHT/ISIS spectrum of Smith & Gallagher (2001).

Cluster F has fainter magnitudes than cluster L in the near-IR and our SpeX data, taken simultaneously with cluster L through the same slit, have a lower signal-to-noise ratio. As a consequence, the χ^2 -curves for cluster F have lower contrast and a broader minimum than those for cluster L. Based on the current data and SSP models, we derive a conservative age range of 15 to 50 Myr for cluster F. The CO bands around $1.6 \mu\text{m}$ and CN bands of the 60 Myr model are uncomfortably weak compared to the observations. The near-IR age range overlaps with the younger of the optical ages from previous studies (Table 2).

In Fig. 13, optical spectra obtained with WHT/ISIS (Smith & Gallagher 2001) and HST/STIS (Smith et al. 2006) are shown. The model displayed corresponds to the best fit to the SpeX spectrum (34 Myr). $R_V = 3.3$ is chosen for a best match to the slope of the STIS spectrum. The STIS spectrum can be matched reasonably well together with the SpeX spectrum. In agreement with results from the SpeX data restricted to short wavelengths, a direct fit to the STIS spectrum alone favours the younger of the ages in the range already indicated. If future improvements of the model inputs lead to stronger near-IR molecular bands at older ages, a more satisfactory match between optical and near-IR ages might be obtained (see Sect. 5.1).

No combination of A_V and R_V provides a satisfactory fit to the more extended combined energy distribution of the SpeX and ISIS data. Efforts to improve the models should be accompanied with new observations of cluster F. Indeed, the direct comparison of the HST/STIS and WHT/ISIS spectra shows differences in the energy distribution, in the absorption features and in the strength of the nebular emission lines (Fig. 13). Considering the wealth of small scale structure around cluster F (McCradly et al. 2005, Bastian et al. 2007), it is not surprising that optical spectra taken one with HST/STIS, the other from the ground differ. The near-IR SpeX spectrum, taken under poor seeing conditions through a relatively broad slit, covers a different area again. The ground based data could be contaminated by emission from younger stars on a neighbouring line of sight, which would also explain the presence of weak emission lines. The complex dust configuration could produce an obscuration law that differs from the ones we have explored here.

4.4. Luminous masses of clusters L and F

Based on the above results, we may estimate the luminous masses of clusters L and F and compare them with dynamical mass estimates. We adopt the cluster magnitudes of McCradly & Graham (2007), and assume a distance to M 82 of 3.6 Mpc. We correct these magnitudes for extinction with the simplifying assumption that our measurement of the reddening indeed translates into extinction as in the dust screen model of Cardelli et al. (1998). In Fig. 14, the measured F160W magnitudes (which depend on age through the age-dependent estimate of extinction) are compared to predictions for single stellar populations with total stellar masses equal to the dynamical masses of Table 2. Our results for cluster F are consistent with previous work: the cluster indeed seems overluminous. At the favoured age of 34 Myr, it is a factor of 2 more luminous than the prediction based on a Salpeter IMF and on a mass of $1.3 \times 10^6 M_\odot$. For cluster L, the luminous and dynamical masses agree.

4.5. Clusters 1a and 1c

Because of poor seeing at the time of the observations, the spectra of clusters 1a and 1c are severely blended and only a combined spectrum has been extracted finally. It displays all the strong molecular bands typical of luminous red supergiants.

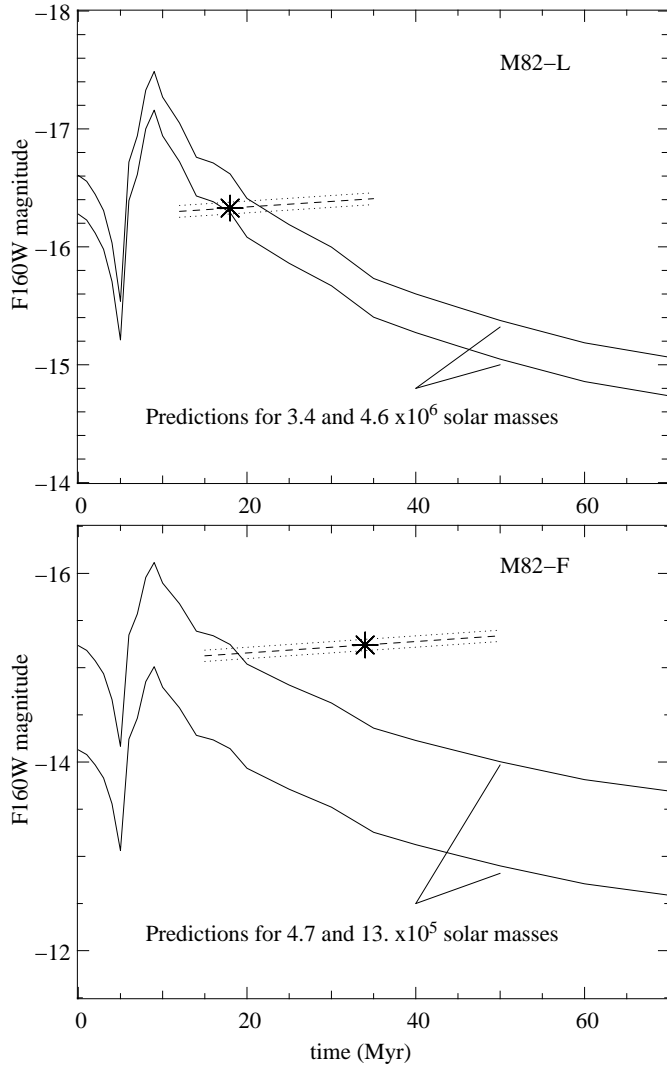


Fig. 14. Absolute dereddened magnitudes of clusters L (top) and F (bottom). The asterisk shows the values favoured based on the near-IR analysis; dotted and dashed lines show the range of acceptable values. The solid lines are predictions, for masses that bracket the range of dynamical masses given in Tab. 2. A Salpeter IMF ($0.1\text{--}120 M_{\odot}$) is assumed.

Figure 15 shows the spatial profiles measured along the slit in two spectral orders, around $1.05 \mu\text{m}$ and around $2.15 \mu\text{m}$. The relative contributions of clusters 1a and 1c are similar at all extracted wavelengths, suggesting either similar ages for both clusters or a fortuitous compensation of an age difference with a difference in extinction. Therefore, we explore single-age population models before considering more complex combinations.

When fitting the spectrum with synthetic spectra of single-age populations (Fig 16), the residuals show that the global curvature of the observed near-IR energy distributions are not matched quite as well as in the case of cluster L or cluster F. The best fitting models are peaked in the H band more than the data. The residuals are of the order of 10% only. Considering the high extinction towards the observed sources ($A_V \sim 5$), we cannot exclude that such a difference may be due to an inade-

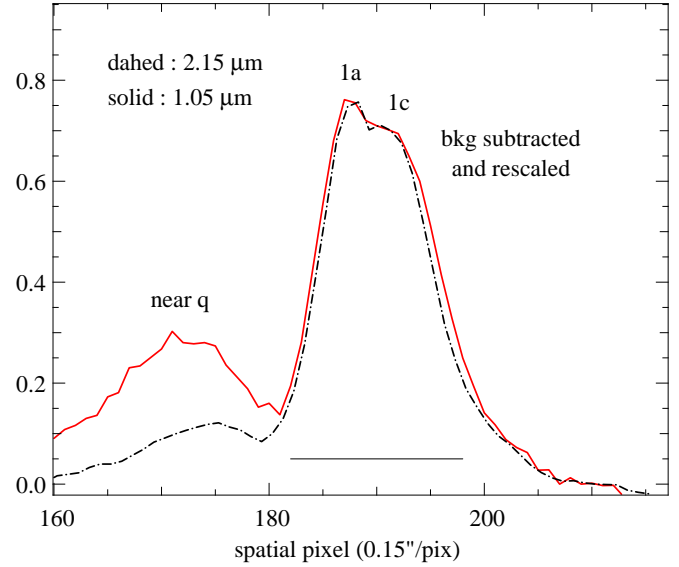


Fig. 15. Spatial profiles across clusters 1a and 1c along the slit of the SpeX spectrograph (after background subtraction). The extracted aperture is indicated.

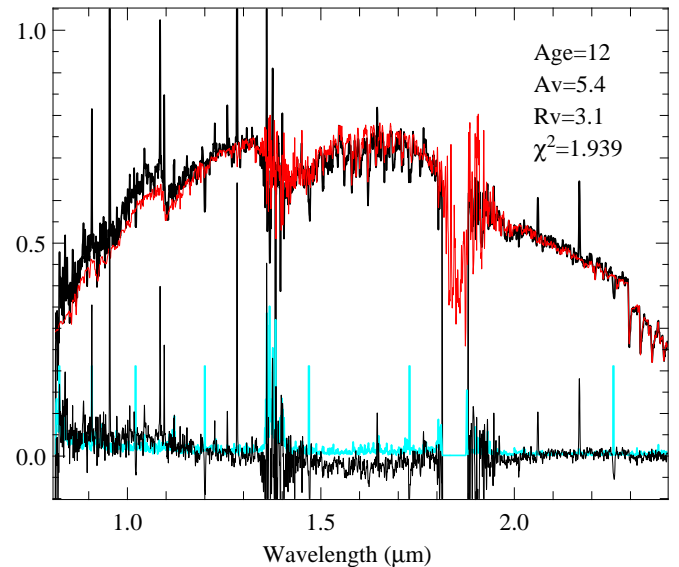


Fig. 16. Best fit to the combined near-IR spectrum of clusters 1a and 1c with a single-age model. The residuals are shown in black, the noise spectrum in cyan (light grey). The weights are similar to those shown for clusters F and L, except that they also mask emission lines. The data and the model have been smoothed with a gaussian kernel for display (FWHM= 10 \AA), and the plotted noise spectrum takes this smoothing into account.

quacy of the adopted extinction law. An excellent fit is obtained when the extinction curve is modified with an *ad hoc* second order polynomial (which takes values between 1 and 1.1).

Figure 17 shows how the reduced χ^2 varies with model age, depending on the wavelength range used to constrain the fit. The spectrum favours ages between 9 and 30 Myr, i.e. the ages at which the red supergiant features in the model spectra are strongest. The thick grey curve (green in the colour version of

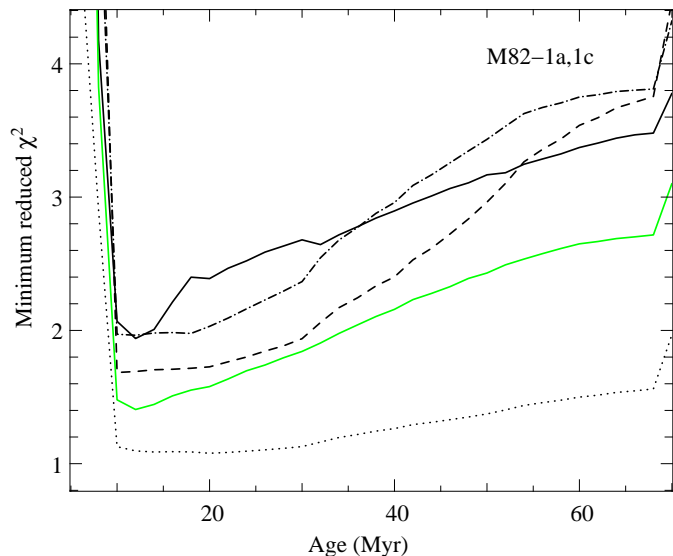


Fig. 17. χ^2 constraints on the age of clusters 1a and 1c. **Solid:** fit of the combined spectrum, performed using all available wavelengths, with weights similar to those used for clusters L and F. **Dashed:** wavelengths restricted to the H and K windows. **Dotted (dot-dashed):** wavelengths restricted to the H window (K window). **Thick solid, green (or grey):** fit to all the available wavelengths but with a modified extinction law.

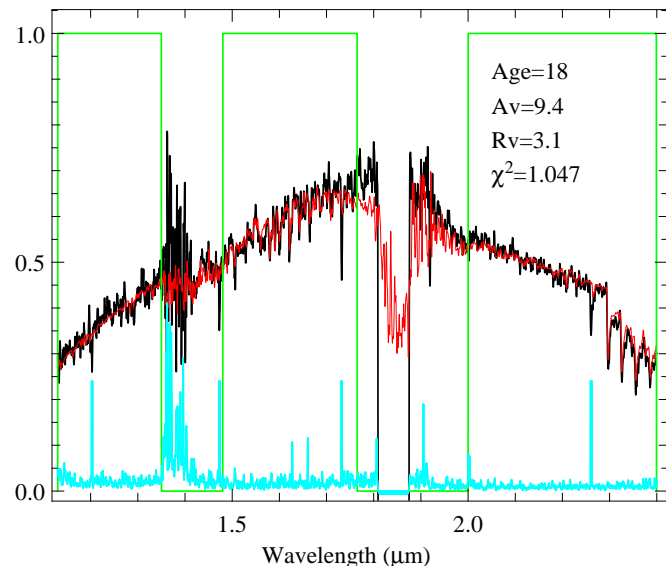


Fig. 19. Best fit to the near-IR spectrum of cluster z. The data and the model have been smoothed with a gaussian kernel for display (FWHM=12 Å), and the plotted noise spectrum takes this smoothing into account.

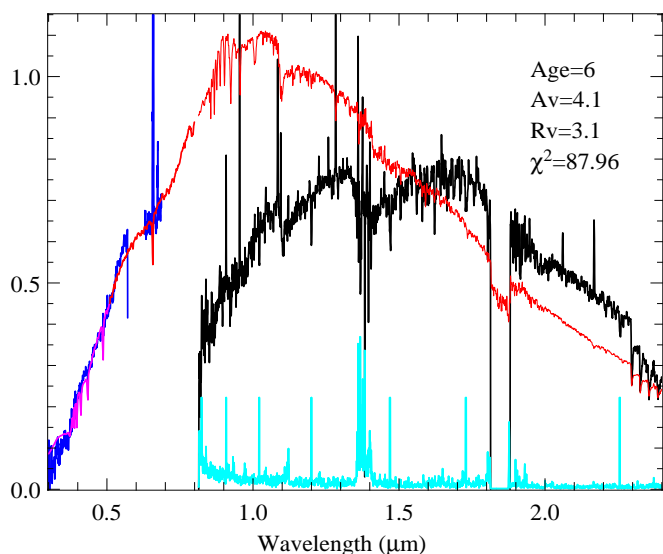


Fig. 18. Comparison of the combined SpeX spectrum of clusters 1a and 1c (black) with a model spectrum (red) based on the age and extinction derived from the HST/STIS spectrum of cluster 1a by Smith et al. (2006): age=6.4±0.5 Myr, E(B-V)=1.35±0.15, $R_V=3.1$. The HST/STIS spectrum of 1a is shown in blue. Within the framework of the population synthesis models of this paper, an age this young is not compatible with the near-IR data.

the figure) is obtained with the modified extinction law: the value of the best χ^2 is reduced but the behaviour with age is otherwise unchanged.

The analysis of the HST/STIS spectrum of cluster 1a by Smith et al. (2006) led to an age of 6 to 7 Myr with E(B-

V)=1.35 and $R_V=3.1$ (we will refer to these estimates as the STIS-parameters below). An age this young is excluded in the framework of our near-IR analysis (Fig. 18): at ages younger than 9 Myr, the stellar evolution tracks of Bressan et al. (1993) do not allow cool supergiants to contribute enough to explain the deep molecular bands we see.

Could two-component models offer a satisfactory solution to this discrepancy? In other words, could a model for cluster 1a based on the STIS-parameters be combined with an older model for cluster 1c in such a way as to match the SpeX data? Within our current setting, the answer is no. The difference in colour between the model shown in Fig. 18 and the SpeX spectrum is incompatible with the small wavelength dependence of the spatial profile across the two clusters along the SpeX slit. The profile also excludes a solution in which an older, highly reddened cluster 1c would outweigh a bluer contribution from cluster 1a by large factors.

Our interpretation of the above discrepancy between optical and near-IR ages is that it is due to an inadequacy of the adopted set of stellar evolution tracks. Despite the impressive mismatch in Fig. 18, the difference between derived optical and near-IR ages is actually small. Between ages of 5 Myr and 10 Myr, the evolution in the ratio between red and blue stars is extremely rapid, and therefore also particularly model dependent. Fig. 2 of Fioc & Rocca-Volmerange (1997) shows that the predicted rapid transition from blue to red (V-K) colour occurs about 3 Myr earlier with the tracks of Meynet et al. (1994), used by Smith et al. (2006), than with those of Bressan et al. (1993), used here. Tracks that include stellar rotation, or tracks with slightly different metallicities, also modify the time at which first red supergiants appear by a few Myr.

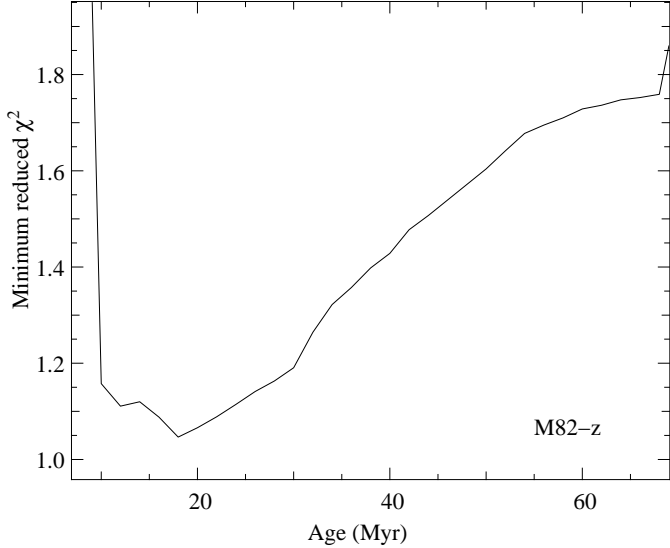


Fig. 20. χ^2 constraints on the age of cluster z , using all near-IR wavelengths indicated by the rectangular weight function in Fig. 19.

4.6. Cluster z

Because of the extreme extinction towards cluster z , we were able to extract its SpeX spectrum only for $\lambda > 1.13 \mu\text{m}$. Figures 19 and 20 show the best fit obtained and the corresponding χ^2 curve. The near-IR constraints on age are similar to those obtained for cluster L and 1a: the molecular bands are strong and this selects ages at which the contributions of luminous red supergiants are important. Ages between 10 and 30 Myr are favoured. A closer look at the fits to the CO bands in the H and K window shows that even these young models produce CO bands that are marginally too weak compared to the data. Ages older than 40 Myr are excluded in the framework of our current models. Clearly, cluster z belongs to the very youngest objects in region B of M82.

It is worth noting that the energy distribution through the near-IR range is extremely well reproduced with the extinction law of Cardelli et al. (1989), despite the high optical depth ($A_V \simeq 9.4$ if $R_V = 3.1$).

5. Discussion

5.1. Near-IR modelling

We have shown that it is possible to obtain very good representations of the near-IR spectra of young massive star clusters. The near-IR ages summarised in Table 2, however, do not always agree with previous optical ages. For the M82 clusters under study, a general trend seems to apply: the near-IR spectra display deep molecular bands, and as a result they point to model ages at which the contributions of luminous red supergiants is important.

The input that most strongly affects the red supergiant contributions at any given age is the adopted set of evolutionary tracks. At ages between 5 and 100 Myr, large differences between the predictions for various available sets are obvious

in colour plots, colour-magnitude diagrams and optical spectra (Fioc & Rocca-Volmerange 1997, Bruzual & Charlot 2003, Levesque et al. 2005, González Delgado et al. 2005). The tracks of the Geneva group (Schaller et al. 1992, Meynet et al. 1994, non-rotating tracks of Meynet & Maeder 2003) produce more and cooler red supergiants at young ages (6–20 Myr) than those of the Padova group, used here. Near-IR models based on the Geneva tracks may well be able reconcile the optical and near-IR ages of cluster M82-1a. Stronger red supergiant contributions are also obtained at a variety of ages with tracks that assume newborn stars rotate (Meynet & Maeder 2000, 2003; Vázquez et al. 2007). Along rotating tracks, the stars tend to spend more time in redder parts of the HR-diagram, the red supergiants evolve at higher luminosities and lower (average) surface gravities, and they have strongly enhanced surface abundances of nitrogen. Both optical and near-IR studies would be affected by these changes.

The second model input of importance for stellar population synthesis is the spectral library. In Sect. 2.1, we noted that until the stellar atmosphere models are able to properly reproduce the extended spectra of individual red supergiants, the values of T_{eff} and $\log(g)$ assigned to individual stars will remain uncertain. They are affected by metallicity, detailed surface abundances, microturbulence and other model atmosphere ingredients. As an illustration of the sensitivity of age dating techniques to these inputs we have computed SSP models in which the spectral sequences of Fig. 1 were shifted up (case A) or down (case B) in g (by 0.4 dex for class Ia, 0.2 dex for class Iab). When assigned gravities are larger (case B; expected if microturbulent velocities are large), spectra of the more luminous sequences are used with larger weights and over a larger range of ages than when assigned gravities are small (case A). The strongest effect is a prediction of stronger CN bands with larger assigned gravities.

We confronted the resulting SSP spectra with observations of cluster F, for which the bluer parts of the near-IR spectrum (predominantly shaped by CN bands) indicated slightly younger ages than the H and K band spectra (Fig. 12). This situation suggested that models with stronger CN bands would provide a better global fit. As expected, case B models led to a wavelength independent near-IR age of 25–30 Myr, while case A made it impossible to match CN and CO bands simultaneously.

This test shows that with the data quality achievable today we are sensitive to spectral differences between *luminosity subclasses*, and it will be useful to continue to include this distinction in future population synthesis models.

The derived ages are expected to be sensitive also to the adopted T_{eff} scale. Assigned temperatures rise by up to 300 K when the microturbulence parameter is increased to 10 km s^{-1} , but (based on a very preliminary exploration of a new series of theoretical spectra) they drop by similar amounts when switching from the solar abundances of Anders & Grevesse, used here (see LHLM07), to those of Asplund et al. (2005).

In view of the above, it is clear that it will be necessary to reassess the cluster data with a wider range of models. The large systematic errors due to the choice of a particular model,

which are not included in Table 2, can then be quantified and reduced by selecting the subset of models providing satisfactory simultaneous fits to both the optical and the near-IR data.

5.2. Stochastic fluctuations

The issue of stochastic fluctuations is the result of the contrast between the small fractional number of bright stars in a stellar population and their large contribution to the luminosity (Girardi & Bica 1993, Santos & Frogel 1997, Lançon & Mouhcine 2000³, Cerviño & Luridiana 2006). Table 3 lists the *average* relative and absolute numbers of red supergiant stars in synthetic single-age populations of total mass $10^6 M_{\odot}$, as well as the contribution of these stars to the flux at $1 \mu\text{m}$ and $2.2 \mu\text{m}$. Note that these numbers depend on the shape of the IMF. Poisson statistics tell us that the r.m.s dispersion in the actual number of red supergiants between single clusters of that mass equals the square root of the average number. In the K band, the red supergiants are so much more luminous than other coeval stars that these variations translate almost directly into dispersions in the fluxes (Lançon & Mouhcine 2000). For colours such as V-K or Z-K, fluctuations are also due partly to varying numbers of luminous blue stars. When average numbers are small (< 10), the predictions can be off-set from the mean or multimodal: the colours vary wildly depending on whether or not a handful of massive stars happen to be in a red or in a blue phase of their evolution.

Table 3 tells us it is necessary to work with clusters of $\sim 10^6 M_{\odot}$ or more, if one wishes to test detailed model ingredients (unless large samples of clusters are available for a statistical analysis). For instance, at an age of 30 Myr a cluster of $\sim 10^6 M_{\odot}$ will contain 260 ± 16 red supergiants, that will on average provide 85 % of the K band flux. Clearly, the ~ 6 % fluctuations in the red supergiant numbers (combined with fluctuations in the numbers of blue stars) will produce a spread in colours such as V-K that make it impossible to test the small differences in average properties resulting from conservative changes in the IMF.

The differences between evolutionary tracks are much larger than those associated with changes in the IMF. We expect that at least some of these will be testable with individual clusters more massive than a few $10^5 M_{\odot}$. Detailed computations with the various sets of tracks now available will be needed in order to verify this statement. As a general rule, even with masses around $10^6 M_{\odot}$, the existence of the fundamental stochastic limitation must be kept in mind.

6. Conclusion

Using new synthetic spectra of single stellar populations that extend to $2.5 \mu\text{m}$ and include red supergiant spectra at resolution $\lambda/\delta\lambda \simeq 750$, we have analysed the near-IR spectra of a few of the most massive star clusters in the starburst galaxy M 82.

We demonstrate that very good fits to all the near-IR photospheric features seen at this resolution can now be obtained. In

particular, the new synthetic spectra can be used for a precise subtraction of the stellar background in emission line studies. The models also significantly improve predictions of the low resolution energy distribution around $1 \mu\text{m}$ over those based on previous stellar libraries. Further improvements around $1 \mu\text{m}$ are to be expected from the inclusion of stars warmer than 5000 K in the library of near-IR spectra used here.

Between ages of 10 and 60 Myr, we have found that the degeneracy between age and extinction is essentially perfect in near-IR broad band photometry (Z,Y,J,H,K), when the extinction law of Cardelli et al. (1989) is used. A simultaneous fit of the near-IR spectra *and* the optical + near-IR energy distribution was obtained for cluster M82-L, and this required a modified extinction law (e.g. the law of Cardelli et al., 1989, with $R_V < 3.1$). This new evidence for non-standard extinction laws towards star clusters in starburst galaxies, which is not surprising considering the very inhomogeneous spatial distribution of the dust in these objects, is an additional difficulty in any attempt to derive ages from photometry alone. The use of extended spectra allows to constrain both the ages and the shape of the extinction law. It is worth recalling, however, that a given shape of the extinction law can correspond to a variety of values of the total amount of obscuration (e.g. Witt & Gordon 2000).

A table of red supergiant numbers and flux contributions has been provided. We argue that the stochastic nature of the stellar mass function must be kept in mind at all cluster masses, but that with masses above $10^5 M_{\odot}$ the analysis of individual extended spectra nevertheless allows us to test *selected* parameters of the population synthesis models. For instance, we expect it will be possible to exploit the largest differences between various sets of current stellar evolution tracks (e.g. tracks for rotating and for non-rotating stars). But we discourage attempts to test the shape of the upper IMF unless cluster mass approaches $10^6 M_{\odot}$.

The absolute ages derived from the near-IR spectra depend on model parameters that are still highly uncertain, to a large part because the physics of red supergiants (evolution, spectra) are particularly complex. More work on the stellar models and more confrontations with star cluster data will be needed. Care needs to be taken in matching the apertures of multi-wavelengths observations. It is promising that data quality now allows us to exploit “details” that were neglected until now, such as the differences between spectra of supergiants of class Ia, Iab and Ib/II.

The near-IR ages found with the current model assumptions for the observed IR-bright clusters in M 82 are concentrated between 9 and 35 Myr. Indeed, their spectra display deep bands of CN and CO, and therefore favour the model ages at which the contributions of luminous red supergiants are strongest. Cluster F, with weaker bands, is the oldest cluster of our sample. In most cases, the near-IR molecular bands of the models at the ages derived from *optical* studies are marginally acceptable or too weak. Changing the adopted evolutionary tracks or the parameters assigned to the spectra of the input stellar library can result in deeper near-IR bands over a wider range of ages. Work is in progress to perform these tests, which should in time al-

³ On p. 35 in that article, divide by l instead of L in the second expression given for σ_L/L .

Table 3. Average numbers and flux contributions of red supergiant stars in single age populations containing $10^6 M_{\odot}$ of stars. Is counted as a red supergiant any star with an initial mass above $7 M_{\odot}$ and an effective temperature below 4900 K. The IMFs are from Salpeter (1955) and Kroupa (1993). The lower mass cut-off is $0.1 M_{\odot}$ for the upper lines, $0.6 M_{\odot}$ for lower lines.

Age (Myr)	Absolute number (Salpeter)	Fractional number (Salpeter)	Fractional contribution at $1 \mu\text{m}$ (Salpeter)	Fractional contribution at $2.2 \mu\text{m}$ (Salpeter)	Absolute number (Kroupa)	Fractional number (Kroupa)	Fractional contribution at $1 \mu\text{m}$ (Kroupa)	Fractional contribution at $2.2 \mu\text{m}$ (Kroupa)
8	60	$2.0 \cdot 10^{-3}$	28 %	44 %	40	$1.8 \cdot 10^{-3}$	27 %	43 %
10	150	$5.2 \cdot 10^{-3}$	72 %	87 %	100	$4.9 \cdot 10^{-3}$	68 %	85 %
30	260	$8.3 \cdot 10^{-3}$	64 %	86 %	220	$1.0 \cdot 10^{-2}$	59 %	84 %
60	360	$1.3 \cdot 10^{-2}$	49 %	73 %	340	$1.7 \cdot 10^{-2}$	46 %	70 %
8	120	$2.4 \cdot 10^{-2}$	28 %	44 %	60	$9.1 \cdot 10^{-3}$	27 %	43 %
60	730	$1.5 \cdot 10^{-1}$	49 %	73 %	570	$8.6 \cdot 10^{-2}$	46 %	71 %

low us to select the theoretical model inputs most appropriate for the analysis of star clusters in starburst galaxies.

Acknowledgements. The authors thank P.R. Wood, P. Hauschildt, W.D. Vacca, N. Förster Schreiber and R. O’Connell for fruitful discussions in the preparation of this work.

References

- Alonso-Herrero, A., Rieke, G.H., Rieke, M.J. & Kelly, D.M. 2003, AJ 125, 1210
- Anders, E., & Grevesse, N. 1989, *Geochim. Cosmochim. Acta* 53, 197
- Asplund, M., Grevesse, N., & Sauval, A.J. 2006, in *Cosmic Abundances as Records of Stellar Evolution and Nucleosynthesis*, T.G. Barnes, III, & F.N. Bash (eds.), ASP Conf. Ser. 336, 25
- Bastian, N., Konstantopoulos, I., Smith, L.J. et al. 2007, MNRAS, 379, 1333
- Bressan, A., Fagotto, F., Bertelli, G., & Choisi, C. 1993, A&AS 100, 647
- Bruzual, G. & Charlot, S. 2003, MNRAS 344, 1000
- Cardelli, J.A., Clayton, G.C. & Mathis, J.S. 1989, ApJ 345, 245
- Cenarro, A.J., Cardiel, N., Gorgas, J. et al. 2001, MNRAS 326, 959
- Cerviño, M., & Luridiana, V. 2006, A&A 451, 475
- Cushing, M.C., Vacca, W.D., & Rayner, J.T. 2004, PASP 116, 362
- de Grijs, R., O’Connell, W.O. & Gallagher III, J.S. 2001, AJ 121, 768
- Elmegreen, B.G. 2006, ApJ 648, 572
- Fioc, M. & Rocca-Volmerange, B. 1997, A&A 326, 950
- Fioc, M., & Rocca-Volmerange, B. 1999, astro-ph/9912179
- Förster Schreiber, N.M., Genzel, R., Lutz, D., Kunze, D., & Sternberg, A. 2001, ApJ 552, 544
- Gallagher, J.S. & Smith, L.J. 1999, MNRAS 304, 540
- Girardi, L., & Bica, E. 1993, A&A 274, 279
- González Delgado, R.M., Cerviño, M., Martins, L.P., Leitherer, C., & Hauschildt, P.H. 2005, MNRAS 357, 945
- Gray, R.O., Graham, P.W., & Hoyt, S.R. 2001, AJ 121, 2159
- Ivanov, V.D., Rieke, M.J., Engelbracht, C.W. et al. 2004, ApJS 151, 387
- Kroupa, P., Tout, C.A., & Gilmore, G. 1993, MNRAS 262, 545
- Lançon, A. & Rocca-Volmerange, B. 1996, NewA 1, 215
- Lançon, A. & Wood, P.R. 2000, A&AS 146, 217
- Lançon, A., & Mouhcine, M. 2000, in *Massive Stellar Clusters*, ed. A. Lançon, & C.M. Boily, ASP Conf. Ser. 211, 34
- Lançon, A., & Mouhcine, M. 2002, A&A 393, 167
- Lançon, A., Hauschildt, P., Ladjal, D. & Mouhcine, M., 2007 a, A&A, 468, 205 (LHLM07)
- Lançon, A., Gallagher, J.S., de Grijs, R. et al. 2007 b, in *Stellar Populations as Building Blocks of Galaxies*, Vazdekis, A. & Peletier, R.F., eds. (Cambridge University Press), IAUS 241, 152
- Larsen, S.S. 2006, in *Planets to Cosmology: Essential Science in the Final Years of the HST*, ed. M. Livio & S. Casertano (Cambridge Univ. Press), STScI Symp. Series 18, 35
- Lejeune, T., Cuisinier, F., & Buser, R. 1998, A&AS 130, 65
- Levesque, E.M., Massey, P., Olsen, K.A.G. et al. 2005, ApJ 628, 973
- Levesque, E.M., Massey, P., Olsen, K.A.G. et al. 2006, ApJ 645, 1102
- Maeder, A., & Meynet, G. 2001, A&A 373, 555
- Maraston, C. 2005, MNRAS 362, 799
- McCraday, N., Gilbert, A.M., & Graham, J.R. 2003, ApJ 596, 240
- McCraday, N., Graham, J.R. & Vacca, W.D. 2005, ApJ 621, 278
- McCraday, N., & Graham, J.R. 2007, ApJ 663, 844
- McGregor, P., Hart, J., Downing, M., Hadley, D., & Bloxham, G. 1994, in *Infrared Astronomy with Arrays, The Next Generation*, ed. I.S. McLean, Astroph. and Sp. Sc. Lib. 190, 299
- Meurer, G.R., Heckman, T.M., Leitherer, C. et al. 1995, AJ 110, 2665
- Meyer, M.R., Edwards, S., Hinkle, K.H., & Strom, S.E. 1999, ApJ 508, 397
- Meynet, G., Maeder, A., Schaller, G., Schaerer, D., & Charbonnel, C. 1994, A&AS 103, 97
- Meynet, G. & Maeder, A. 2000, A&A 361, 101
- Meynet, G. & Maeder, A. 2003, A&A 404, 975
- Mouhcine, M., & Lançon, A. 2002, A&A 393, 167
- Mutchler, M., Bond, H.E., Christian, C.A. et al. 2007, PASP 119, 1
- O’Connell, R.W., & Mangano, J.J. 1978, ApJ 221, 62
- Oliva, E., Origlia, L., Kotilainen, J.K., & Moorwood, A.F.M. 1995, A&A 301, 55
- Origlia, L., Moorwood, A.F.M., & Oliva, E. 1993, A&A 280, 536
- Origlia, L., Ferraro, F.R., Fusi Pecci, F., & Oliva, E. 1997, A&A 321, 859
- Pickles, A.J. 1998, PASP 110, 863
- Rayner, J.T., Toomey, D.W., Onaka, P.M. et al. 2003, PASP 115, 362
- Rieke, G.H. & Lebofsky, M.J. 1979, ARA&A 17, 477
- Rieke, G.H., Loken, K., Rieke, M.J., & Tamblyn, P. 1993, ApJ 412, 99
- Rossa, J., Laine, S., van der Marel, R.P. et al. 2007, AJ 134, 2124
- Salpeter, E.E., 1955, ApJ 121, 161
- Santos, J.F.C., Jr. & Frogel, J.A. 1997, ApJ 479, 764
- Satyapal, S., Watson, D.M., Pipher, J.L. et al. 1997, ApJ 483, 148
- Smith, L. J. & Gallagher, J. S. 2001, MNRAS 326, 1027
- Smith, L.J., Westmoquette, M.S., Gallagher, J.S., III, et al. 2006, MNRAS 370, 513
- Smith, L.J., Bastian, N., Konstantopoulos, I.S. et al. 2007, ApJ 667, L145
- Tsuji, T. 1976, PASJ 28, 543
- Vacca, W.D., Cushing, M.C., & Rayner, J.T. 2003, PASP 115, 389
- Vázquez, G.A., Leitherer, C., Schaerer, D., Meynet, G., & Maeder, A. 2007 ApJ 663, 995
- Wallace, L., Meyer, M.R., Hinkle, K.H., & Strom, S.E. 2000, ApJ 535, 325
- Witt, A.N., & Gordon, K.D. 2000, ApJ 528, 799

List of Objects

- 'M82' on page 2
- 'M82-F' on page 6
- 'M82-L' on page 6
- 'M82-1a' on page 6
- 'M82-1c' on page 6
- 'M82-z' on page 6